

Neuronal growth regulator 1 promotes adipocyte lipid trafficking via interaction with CD36

Ara Yoo¹, Yeonhee Joo¹, Yeongmi Cheon^{1,2} , Sung Joong Lee³, and Soojin Lee^{1,*} 

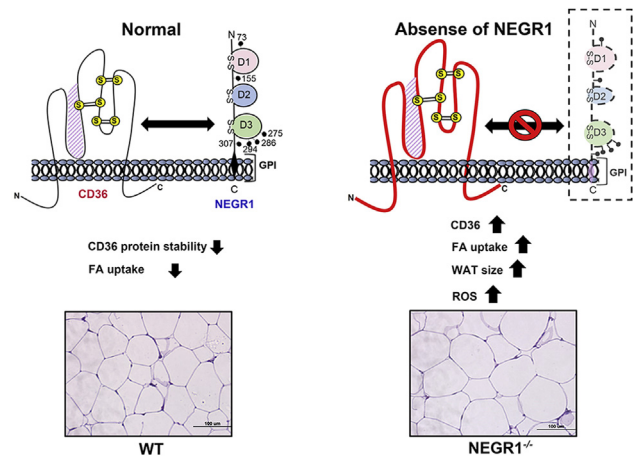
¹Department of Microbiology and Molecular Biology, Chungnam National University, Daejeon, Republic of Korea;

²Gwangju Center, Korea Basic Science Institute (KBSI), Gwangju, Republic of Korea; ³Department of Dentistry, Seoul National University, Seoul, Republic of Korea

Abstract Neuronal growth regulator 1 (NEGR1) is a glycosylphosphatidylinositol-anchored membrane protein associated with several human pathologies, including obesity, depression, and autism. Recently, significantly enlarged white adipose tissue, hepatic lipid accumulation, and decreased muscle capacity were reported in *Negr1*-deficient mice. However, the mechanism behind these phenotypes was not clear. In the present study, we found NEGR1 to interact with cluster of differentiation 36 (CD36), the major fatty acid translocase in the plasma membrane. Binding assays with a soluble form of NEGR1 and in situ proximal ligation assays indicated that NEGR1-CD36 interaction occurs at the outer leaflet of the cell membrane. Furthermore, we show that NEGR1 overexpression induced CD36 protein destabilization in vitro. Both mRNA and protein levels of CD36 were significantly elevated in the white adipose tissue and liver tissues of *Negr1*^{-/-} mice. Accordingly, fatty acid uptake rate increased in NEGR1-deficient primary adipocytes. Finally, we demonstrated that *Negr1*^{-/-} mouse embryonic fibroblasts showed elevated reactive oxygen species levels and decreased adenosine monophosphate-activated protein kinase activation compared with control mouse embryonic fibroblasts. **Based on these results, we propose that NEGR1 regulates cellular fat content by controlling the expression of CD36.**

Supplementary key words obesity • adipose tissue • fatty acid/transport • CD36 • lipid rafts • proximal ligation assay • protein-protein interaction • ROS • AMPK activation • diabetes

Obesity is characterized by an abnormal increase in intracellular fat accumulation (1), and it has become the most common global disease (2). Exogenous supply of fatty acids seems to be the preferred source for cellular lipids compared with their de novo synthesis in proliferating fibroblasts as well as in HeLa cells (3), suggesting that the regulation of fatty acid uptake is important for lipid balance. Long-chain fatty acids (LCFAs) not only contribute to cellular metabolic energy generation and storage but also have hormone-like properties that



regulate gene expression (4). Several protein groups including cluster of differentiation 36 (CD36)/fatty acid translocase, fatty acid transporter proteins (FATPs), and plasma membrane fatty acid-binding protein (FABPpm) are known to transport LCFAs (5, 6). CD36 plays a major role in LCFA uptake in metabolic tissues, including adipose tissues, cardiomyocytes, and skeletal muscle myocytes (7), contributing to more than 50% of the rate of fatty acid uptake in these tissues (8).

As a scavenger receptor class B-2 protein, CD36 is an integral membrane protein with a hairpin-like topology and two transmembrane regions (7). Furthermore, CD36 is associated with membrane rafts, and CD36-mediated fatty acid uptake depends on the integrity of membrane rafts in adipocytes (9). CD36 is ubiquitously expressed in diverse mammalian cell types, which include skeletal and cardiac myocytes, macrophages, endothelial cells, adipocytes, and gut epithelial cells (10). Its functions are primarily related to lipid metabolism and innate immunity, and its dysregulation has been reported in various human pathologies, including atherothrombotic diseases, obesity, diabetes, cancer, and Alzheimer's disease (7). Activation of adenosine monophosphate-activated protein kinase (AMPK) is related to the CD36-mediated LCFA uptake

*For correspondence: Soojin Lee, leesoojin@cnu.ac.kr.

pathway and fatty acid utilization in skeletal muscle (11).

Neuronal growth regulator 1 (NEGRI) consists of three C2-type immunoglobulin domains localized on the extracellular side of plasma membranes. This protein strongly binds membrane lipid rafts via a glycosylphosphatidylinositol anchor. NEGRI functions as a cell-adhesion molecule that plays an important role in neural cell recognition and neurite outgrowth (12). Multiple genome-wide association studies have revealed that genetic alterations in *NEGRI* are associated with obesity (13), intellectual disability (14), schizophrenia (15), depression (16), and Alzheimer's disease (17). We recently reported alterations in the affective behavior of *Negr1*^{-/-} mice (18), implying that NEGRI is closely related to CNS function.

Although NEGRI is highly expressed in the brain (19), it is also expressed in several peripheral tissues, such as subcutaneous adipose tissues and skeletal muscles (HumanProtein Atlas database, <https://www.proteinatlas.org>). In addition, NEGRI is found in different cell types, including adipocytes, myocytes, and endothelial cells, as well as the cells within the nervous system (the Genotype-Tissue Expression database [GTEx] portal, <https://www.gtexportal.org>). We originally identified human NEGRI as a commonly down-regulated gene in various human tumor tissues (12). Subsequent binder analysis unexpectedly revealed the role of NEGRI in intracellular cholesterol trafficking and lipid storage (20). In a recent study, *Negr1*^{-/-} mice also presented substantial enlargement of white adipose tissues (WATs) with increased cell size, further supporting the role of NEGRI in intracellular lipid transport (21). Increased hepatic fat accumulation and skeletal muscle atrophy have also been observed in NEGRI-deficient mice (21). In the present study, NEGRI was found to interact with CD36, increasing our understanding of the role of these proteins in intracellular lipid trafficking and related human diseases.

MATERIALS AND METHODS

Animals, cell culture, and cloning

All animals, including *Negr1*^{+/-} and *Negr1*^{-/-} C57BL6 mice (20), were kept on 12 h light/dark cycles in a controlled environment at 22–24°C and 55% humidity. All animal procedures were approved by the Seoul National University Institutional Animal Care and Use Committee. Mouse embryonic fibroblasts (MEFs), 3T3-L1, and 293T cells (21) were maintained in DMEM (Welgene, Gyeongsan, South Korea) supplemented with 10% FBS (Atlas Biologicals, Fort Collins, CO). SKOV-3 cells were cultured in RPMI 1640 medium (Welgene).

The open reading frame of gene *CD36* was obtained by PCR amplification of the total RNA extracted from 293T cells and subcloned into pKH-3HA (22) or pcDNA3-3FLAG (21) plasmids. Glutathione-S-transferase (GST)-fused deletion constructs of the CD36 extracellular domain were generated using plasmid pEBG (20). To generate the

pcDNA4-FLAG-NEGRI construct, we subcloned *NEGRI* into the pcDNA4/TO vector (Invitrogen, Carlsbad, CA), using restriction enzymes AflIII and XbaI and a 3×FLAG sequence inserted between the signal sequence (positions 1–39) and the remaining *NEGRI* gene sequence (positions 40–314). To obtain SKOV-3-FLAG-NEGRI stable cells, pcDNA4-FLAG-NEGRI was transfected into SKOV-3 cells and selected with zeocin (50 µg/ml; Invitrogen).

Histological analysis and immunofluorescence microscopy

For visualizing target proteins in tissue sections, small sections of various tissues were fixed overnight in 4% paraformaldehyde and embedded in paraffin. Tissue sections were immunostained with the appropriate primary antibodies in PBS, followed by incubation with the fluorescent-linked secondary antibodies, FITC-labeled anti-mouse IgG antibody (Sigma-Aldrich, St. Louis, MO) or Cy3 anti-rabbit IgG antibody (Jackson ImmunoResearch Laboratories, West Grove, PA).

Immunofluorescence microscopy was conducted as previously described (23). Briefly, cells grown on coverslips were either untreated or permeabilized with 0.1% Triton X-100 in PBS for 10 min. After incubation with the appropriate primary antibodies, cells were treated with fluorescent-linked secondary antibodies. Alexa Fluor 594 anti-human IgG antibody (Invitrogen) was used to detect the Fc-fusion protein. To visualize intracellular lipid droplets, fixed cells were stained with BODIPY 493/503 (2 µM; Thermo Fisher Scientific, Waltham, MA) for 10 min. Imaging was performed on an Olympus BX51 (Tokyo, Japan) microscope and analyzed using ImageJ software (National Institutes of Health, Bethesda, MD).

Gene expression analysis and immunoblotting

To compare gene expression between the peripheral tissues of *Negr1*^{-/-} and *Negr1*^{+/+} C57BL6 mice, liver, skeletal muscle, and epididymal adipose tissues were obtained ($n = 4-8$). To analyze CD36 mRNA expression, total RNA was extracted from tissue samples using a NucleoSpin RNA Extraction kit (Macherey-Nagel, Düren, Germany) and converted into complementary DNA using a SuperScript III Reverse Transcription kit (Invitrogen). Quantitative real-time RT-PCR was performed on a CFX connect™ Real-Time PCR Detection System (Bio-Rad Laboratories, Hercules, CA) with specific primers for CD36 (forward: 5-GCATGAGAATG CCTCCAAACA-3; reverse: 5-CGGAAGTGTGGGCTCATT G-3); GAPDH was used as reference for normalization.

For immunoblotting, tissue samples were homogenized in a lysis buffer (25 mM Tris, pH 7.6, 150 mM NaCl, 50 mM NaF, 1 mM sodium vanadate, 1% NP-40, and 0.1% SDS) and centrifuged at 12,000 *g* for 30 min to remove insoluble materials. Specific antibodies were used to visualize each protein: anti-β-actin, anti-FLAG, and anti-NEGRI (Sigma-Aldrich); anti-hemagglutinin (HA) and anti-CD36 (Santa Cruz Biotechnology, Dallas, TX); anti-GAPDH (Cusabio, Baltimore, MD); and anti-AMPK and antiphosphorylated AMPK (p-AMPK) (Cell Signaling Technologies, Beverly, MA).

Subcellular fractionation and binding assay

Lipid raft fractionation was performed using OptiPrep™ iodixanol (Sigma-Aldrich) (12). Briefly, cell lysates were adjusted to 32% OptiPrep™ and sequentially overlaid with 24% and 20% iodixanol solutions. After centrifugation at 76,000 *g* for 18 h at 4°C, the fraction collected from the top

was designated as no. 1. After tissue lysates were adjusted to 32% OptiPrep™ and overlaid with 24% and 20% iodixanol solutions, endosomal fractionation was carried out using centrifugation at 76,000 *g* for 1 h at 4°C. Plasma membranes were isolated using a Minute™ Plasma Protein Isolation kit (Invent Biotechnologies, Plymouth, MN) according to the manufacturer's instructions.

Immunoprecipitation (IP) was performed following a previously described method (24), with slight modifications. Cells were lysed in a buffer (50 mM Tris, pH 7.4, 250 mM NaCl, 5 mM EDTA, 1% NP-40, 1 mM PMSF, 50 mM NaF, 1 mM Na₃VO₄, and 0.02% NaN₃) supplemented with a protease inhibitor cocktail (Sigma-Aldrich). Then, samples were incubated with 0.75 µg of appropriate antibodies for 3 h at 4°C before incubation with Protein A Sepharose beads (GE Healthcare, Piscataway, NJ). GST-pulldown assays were performed using 1 µg of appropriate antibody or Glutathione-Sepharose 4B beads (GE Healthcare) as described in a previous study (20).

In situ proximity ligation assay

The proximity ligation assay (PLA) was performed on fixed SKOV-3-NEGRI-FLAG cells using Duolink PLA technology reagents (Sigma-Aldrich) according to the manufacturer's protocol. Briefly, fixed cells were first incubated with anti-CD36 and anti-FLAG antibodies for 2 h and then with PLA probes (anti-mouse MINUS and anti-rabbit PLUS, respectively) and Alexa Fluor 488 phalloidin (Invitrogen) for 1 h. After incubation with a ligation solution for 30 min and an amplification solution for 2 h, the cells were mounted in a 4',6'-diamidino-2-phenylindole-containing solution. Imaging was performed using an Olympus BX51 microscope or a TCS

SP5 AOBs confocal microscope equipped with a 63× inverted NX oil lens (Leica Microsystems GmbH, Wetzlar, Germany).

Measurement of fatty acid uptake and cellular reactive oxygen species level

To perform the fatty acid uptake assay, primary adipose cells were isolated from epididymal adipose tissue as described previously (21). After seeding in 96-well plates, cells were incubated with serum-free DMEM for 1 h. Fatty acid uptake was assessed using a Free Fatty Acid Uptake Assay kit (catalog no.: ab176768; Abcam, Cambridge, UK) according to the manufacturer's instructions. Fluorescence signals were measured using a fluorescence microplate reader (Varioskan LUX; Thermo Fisher Scientific) at 485/515 nm.

Cellular reactive oxygen species (ROS) level was measured using a DCFDA (2',7'-dichlorofluorescein diacetate)/H2DCFDA (2',7'-dichlorodihydrofluorescein diacetate) Cellular ROS Assay kit (catalog no.: ab113851; Abcam) as per the manufacturer's instructions. If required, cells were preincubated with hydrogen peroxide (H₂O₂) or oleic acid for 24 h before the assay. Fluorescence signals were measured at 485/515 nm.

RESULTS

Increased CD36 expression in the adipose tissues of *Negr1*^{-/-} mice

Our previous study reported that epididymal WAT was enlarged in *Negr1*^{-/-} mice compared with WT mice (21). To confirm this, we determined the gonadal WAT weight of

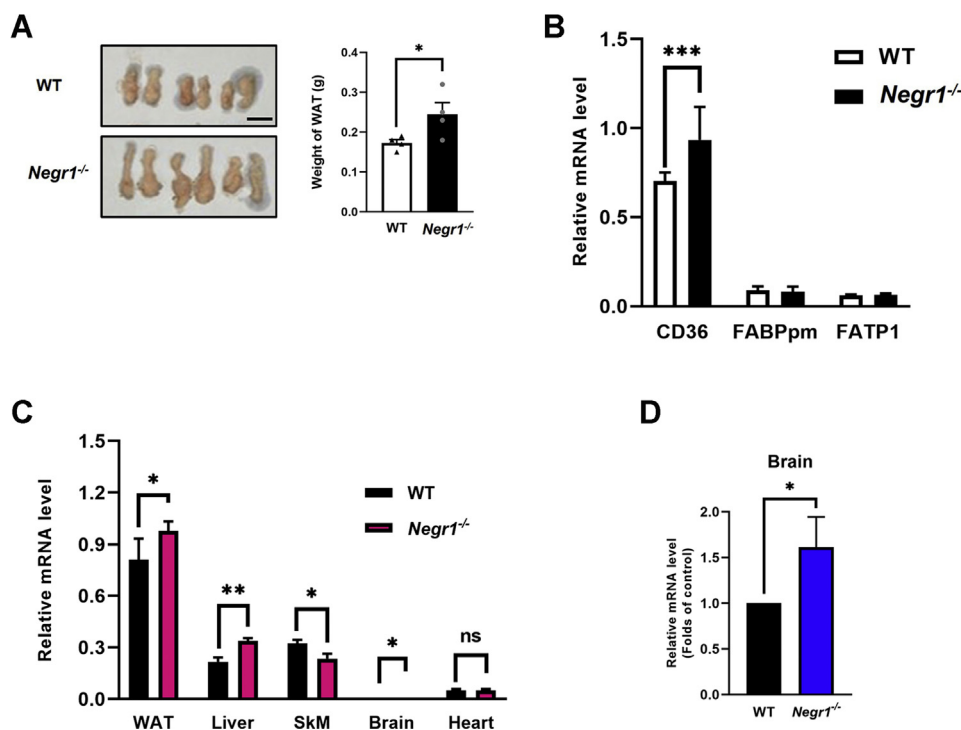


Fig. 1. CD36 expression was upregulated in the WAT of *Negr1*^{-/-} mice. A: Epididymal WATs were dissected from 10-week-old *Negr1*^{+/+} and *Negr1*^{-/-} C57BL6 mice (*n* = 8), and each fat pad weight was determined. The figure shows mean ± SD of individual weights. Bar represents 10 mm. B: Quantitative RT-PCR was performed to measure the mRNA expression levels of CD36, FABPpm, and FATP1 using total RNA obtained from gonadal WAT (*n* = 8). Relative expression was calculated using GAPDH as a reference gene. C: CD36 gene expression was measured by quantitative RT-PCR using WAT, liver, heart, brain, and skeletal muscle (SkM) tissue samples of 10-week-old mice (*n* = 4–7). D: Relative CD36 expression in brain tissues of *Negr1*^{-/-} and WT mice. All experiments were performed in triplicates, and the data are presented as the mean ± SD. **P* < 0.05; ***P* < 0.01; and ****P* < 0.001. ns, not significant.

10-week-old male mice. *Negr1*^{-/-} mice showed approximately 1.4-fold increase in WAT weight ($P = 0.026$) compared with WT mice (Fig. 1A). To investigate which fatty acid transporter is involved in the transport of LCFAs across the cell membrane of adipose tissues, we examined the expression levels of three main transporters, namely CD36, FABPpm, and FATP1, in the gonadal WAT of WT and *Negr1*^{-/-} mice. When quantified using GAPDH as a reference gene, the expression level of CD36 was much higher than that of FABPpm and FATP1, which suggested that CD36 may play an important role in transporting LCFAs in adipose tissues (Fig. 1B). Furthermore, CD36 expression increased significantly (1.3-fold, $P = 0.0007$) in *Negr1*^{-/-} mice compared with WT mice, whereas FABPpm and FATP1 showed no difference (Fig. 1B).

To investigate CD36 expression in other tissues, quantitative RT-PCRs were performed on the mRNAs of WAT, liver, heart, brain, and gastrocnemius (GA) skeletal muscle tissues. The expression of CD36 was approximately 3-fold higher in WAT than in the liver or GA muscle tissues (Fig. 1C). In NEGR1-knockout

mice, CD36 expression increased in liver (1.4-fold) and brain tissues (1.6-fold) but decreased in GA muscle tissue (1.6-fold) (Fig. 1C, D). Overall, our results suggest that the increased WAT weight of *Negr1*^{-/-} mice may be associated with increased expression of CD36, which is the main LCFA transporter in adipocytes.

Interaction of NEGR1 with CD36

Based on earlier findings that both NEGR1 and CD36 contain large extracellular regions and are associated with lipid rafts in the plasma membrane (12, 25, 26), we investigated the possible molecular interaction of NEGR1 and CD36. We first obtained the complementary DNA of *CD36* from the total RNA of 293T cells and generated an HA-tagged CD36 construct using plasmid pcDNA3-HA. After pcDNA3-HA-CD36 and pEGFP-C1-NEGR1 (12) plasmids were transfected into HeLa cells, we performed co-IP using anti-GFP antibodies. Immunoblotting with anti-HA antibody revealed that CD36 was present in the NEGR1-enriched fraction but not in the IgG-enriched control (Fig. 2A). GFP-NEGR1 was

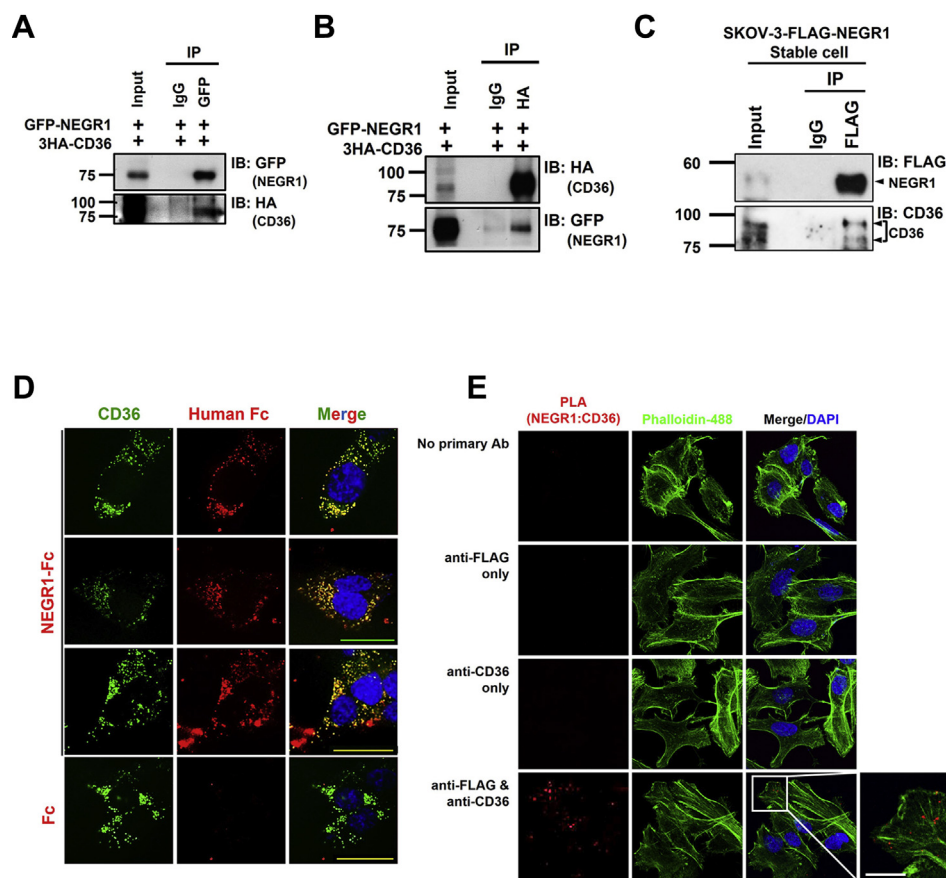


Fig. 2. NEGR1 interacts with CD36. A: Co-IP between transiently expressed HA-CD36 and GFP-NEGR1. After HeLa cells were transfected with HA-CD36 and GFP-NEGR1 plasmids, cell lysates were subjected to IP with anti-GFP antibody. *IgG bands. B: Reciprocal IP using anti-HA antibody. C: IP was performed with SKOV-3-FLAG-NEGR1 stable cells using anti-FLAG antibody. Coisolated CD36 was visualized with anti-CD36 antibody. D: Binding assay using soluble NEGR1-Fc protein. SKOV-3 cells were incubated for 2 h with the conditioned medium of 293T cells expressing NEGR1-Fc or Fc control. Then, cells were immunostained with anti-human Fc and anti-CD36 antibodies. Bar represents 20 μm . E: In situ PLA was performed with SKOV-3-FLAG-NEGR1 cells using Duolink PLA technology. After treatment with anti-CD36 and anti-FLAG antibodies for 2 h, cells were incubated with PLA probes (anti-mouse MINUS and anti-rabbit PLUS, respectively) for 1 h. Cellular actin polymers were stained with Alexa Fluor 488 phalloidin. Bar represents 10 μm .

coisolated with HA-CD36 (Fig. 2B), suggesting an interaction between NEGRI and CD36.

Next, we examined NEGRI and CD36 molecular interaction at the endogenous level using HeLa cell lysates. As no interaction was observed, possibly because of the low IP efficiency of the anti-NEGRI antibody, we performed IP using the SKOV-3-FLAG-NEGRI stable cells. When IP was performed with an anti-FLAG antibody, highly glycosylated forms of CD36 were observed in the NEGRI fraction by immunoblotting with anti-CD36 antibody (Fig. 2B).

To clearly demonstrate that NEGRI-CD36 interaction can occur at the extracellular surface of cell membranes, we performed an *in situ* binding assay using the human Fc-fused secreted form of NEGRI (23). The culture medium of 293T cells transfected with NEGRI-Fc or Fc control plasmids was collected and provided to SKOV-3 cells for incubation for 2 h. After this period, cells were coimmunostained with anti-human Fc antibody (red) and CD36 antibody (green) (Fig. 2C). Whereas the Fc signal was barely observed in control cells treated with Fc-containing medium (fourth row, Fig. 2C), strong Fc signals were visualized in the NEGRI-Fc-treated cells, which overlapped CD36 signals well. These results suggest NEGRI can interact with CD36 at the cell surface.

To verify the NEGRI-CD36 interaction, an *in situ* PLA was performed using SKOV-3-FLAG-NEGRI cells (Fig. 2D). Cells were incubated with anti-FLAG and anti-CD36 antibodies after cell permeabilization, and phalloidin staining was used to examine cell morphology. While no signals were observed in cells treated with a single antibody, clear fluorescent signals were detected in cells treated with both antibodies, indicating NEGRI and CD36 exist in close proximity. In addition, strong fluorescent signals were observed when PLA was performed under nonpermeabilized conditions (Supplemental Fig. S1) demonstrating that NEGRI-CD36 interaction occurs in the cell membrane.

Determination of binding regions of NEGRI and CD36 proteins

NEGRI has a relatively simple structure containing three consecutive C2-type Ig-like domains. In contrast, the extracellular region of CD36 contains only the CLESH (CD36, lysosomal integral membrane protein-2 [LIMP-2], Emp sequence homology; residues 93–155) and proline-rich (243–375) domains (27) (Fig. 3A, B). It was predicted that CD36 contains a lipid binding pocket at residues 127–279 (28), including a hydrophobic patch that might loop down into the plasma membrane (29). To determine the protein regions responsible for CD36-NEGRI interaction, we generated GST-fused CD36 deletion constructs, and each mutant construct was transfected into 293T cells together with the pcDNA4-FLAG-NEGRI plasmid.

As expected, the mutant containing most of the extracellular region of CD36 bound NEGRI in the

GST-pulldown assay (Fig. 3B). The small N-terminal portion of the extracellular region (N1, 30–125) before the peculiar hydrophobic patch successfully interacted with NEGRI. However, the larger construct comprising the hydrophobic region (N2, 30–242) lost the binding activity, which was restored in the N3 mutant (30–375) containing three disulfide bridges. We could not detect NEGRI signals in the N2-enriched fraction even with prolonged exposure. Furthermore, the Δ N1 construct (126–439) was generated, although it did not express well, possibly because of the exposed hydrophobic region.

The NEGRI domains that participate in CD36 binding were detected using GST-fused NEGRI deletion constructs (D1–3, D1–2, D2–3, D1, D2, and D3), which were produced in a previous study using three C2-type Ig-like domains (12). 293T cells were transfected with different NEGRI mutant constructs along with pcDNA3-HA-CD36 plasmids. In the subsequent GST-pulldown assay, the D3 domain showed excellent binding activity to CD36 (Fig. 3C), whereas no binding affinity was found in the other two domains (D1 and D2). Unexpectedly, D1–2 also cofractionated with CD36, possibly because of the sequence similarity between Ig-like domains. Collectively, we suggest that the N-terminal region of CD36 and C-terminal D3 domain of NEGRI play important roles in the interaction between these two proteins.

Colocalization of NEGRI and CD36 in SKOV-3 cells

To examine whether NEGRI and CD36 coexist in cells, we performed immunofluorescence staining. First, SKOV-3-FLAG-NEGRI stable cells were used for immunostaining with or without Triton X-100 treatment. Stably expressed NEGRI was detected with anti-FLAG antibody, whereas endogenous CD36 was visualized using an anti-CD36 antibody. In the presence of 0.1% Triton X-100, both proteins were visualized inside the cells, and these signals overlapped well (upper two rows, Fig. 4A), suggesting their colocalization possibly in endomembrane systems such as the endoplasmic reticulum and endosomes. In nonpermeabilized cells, NEGRI and CD36 were detected in the cell membrane, especially at cell boundaries (lower two rows, Fig. 4A).

We also performed fluorescent immunochemical staining of tissue sections from the mouse brain. Both Negr1 and CD36 proteins were observed in the hippocampal region (Fig. 4B). Although their overall expression patterns appeared to be different, we observed some overlapping areas in this region, supporting the suggestion that NEGRI and CD36 are colocalized in the brain tissue.

Next, we performed a flotation experiment using the OptiPrep™ gradient on 293T cells transfected with HA-CD36 and GFP-NEGRI plasmids. Twelve fractions were obtained, and flotillin-1 was used as the lipid raft marker. Only a minor portion of transiently expressed CD36 protein was detected in the rafts when cells were cotransfected with the enhanced GFP control vector

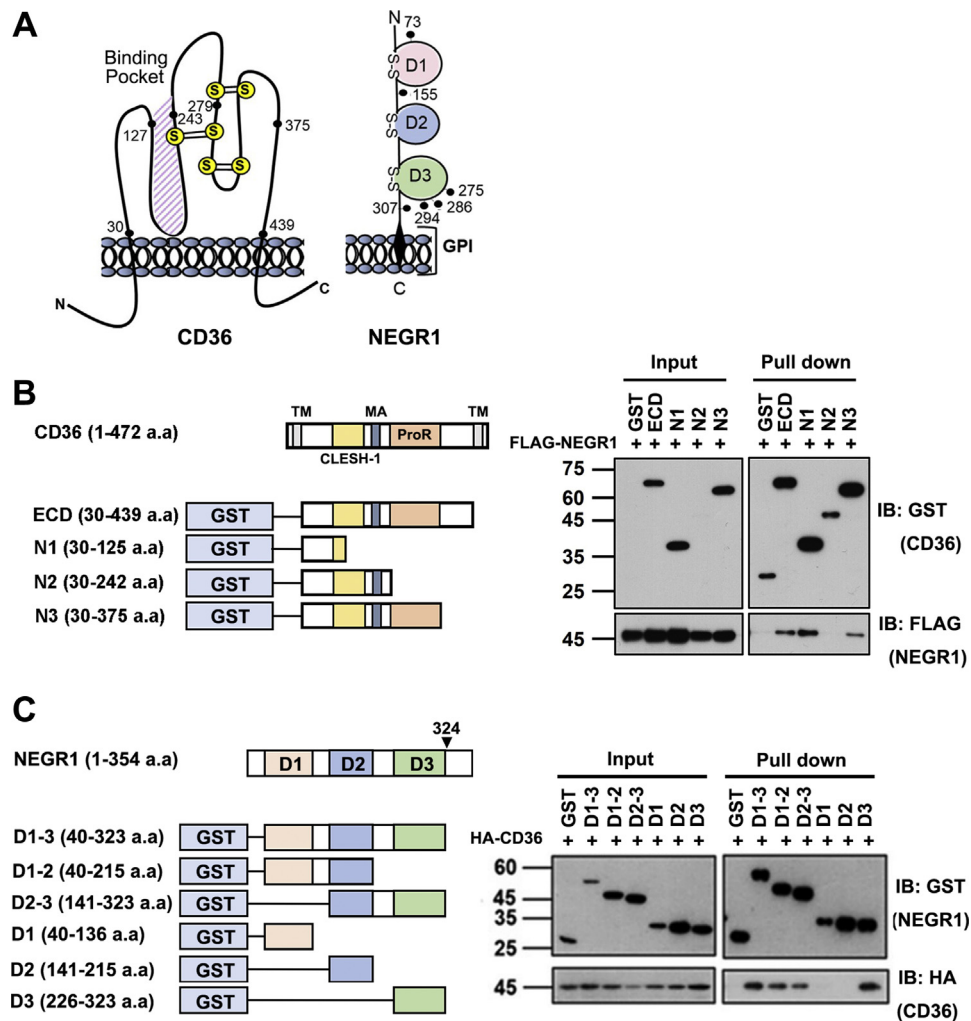


Fig. 3. Determination of important regions for NEGR1-CD36 interaction. A: Schematic diagram of CD36 and NEGR1 structure. Potential N-glycosylation sites were indicated as filled circles. B: Deletion constructs of the CD36 extracellular domain (ECD) were generated as GST-fused form and transfected into 293T cells together with FLAG-NEGR1 plasmid. After GST-pulldown assay, cofractionated NEGR1 was detected using immunoblotting with anti-FLAG antibody. C: 293T cells were transfected with different deletion constructs of GST-NEGR1, together with HA-CD36 plasmid. Then, the cell lysates were subjected to GST-pulldown assay. MA, membrane associated; ProR, proline-rich; TM, transmembrane.

(left, Fig. 4C). The raft-associated CD36 protein was only observed after prolonged exposure. Contrastingly, when GFP-NEGR1 was coexpressed, CD36 appeared in the raft fraction upon short exposure. Our results suggest that NEGR1 may interact with CD36 in the lipid rafts, thus promoting the association of CD36 within these membrane compartments when both proteins are overexpressed.

To determine whether the increased CD36 protein levels in gonadal WAT of *Negr1*^{-/-} mice were accompanied by changes in subcellular protein distribution, we performed cell fractionation using OptiPrep™ density gradient ultracentrifugation. Both CD36 and NEGR1 proteins were highly enriched in the endosomal fractions in WT mice (Fig. 4D, left), whereas the overall CD36 distribution was not changed in *Negr1*^{-/-} mice (Fig. 4D, right). Then, plasma membrane fractions were isolated from the WAT of WT and *Negr1*^{-/-} mice using the Minute™ Plasma Protein Isolation kit. When

normalized to total CD36 levels, the plasma membrane-associated CD36 levels increased in *Negr1*^{-/-} mice by ~1.5-fold, whereas the cytosolic CD36 levels slightly decreased compared with those in WT mice (Fig. 4E). Our data suggest that membrane trafficking of CD36 is facilitated in NEGR1-deficient cells.

Influence of NEGR1 on cellular CD36 protein level

To investigate whether NEGR1 may affect the CD36 protein levels, we cotransfected HA-CD36 and GFP-NEGR1 plasmids into 293T cells. Subsequent immunoblotting revealed that HA-CD36 proteins appeared as two major bands, which may differ in glycosylation status. Although the intensities of both bands decreased gradually in proportion to NEGR1 expression, immature forms (lower band) were more severely affected than the highly glycosylated mature forms (Fig. 5A). To evaluate this phenomenon more clearly, we measured CD36 protein levels in the presence of cycloheximide

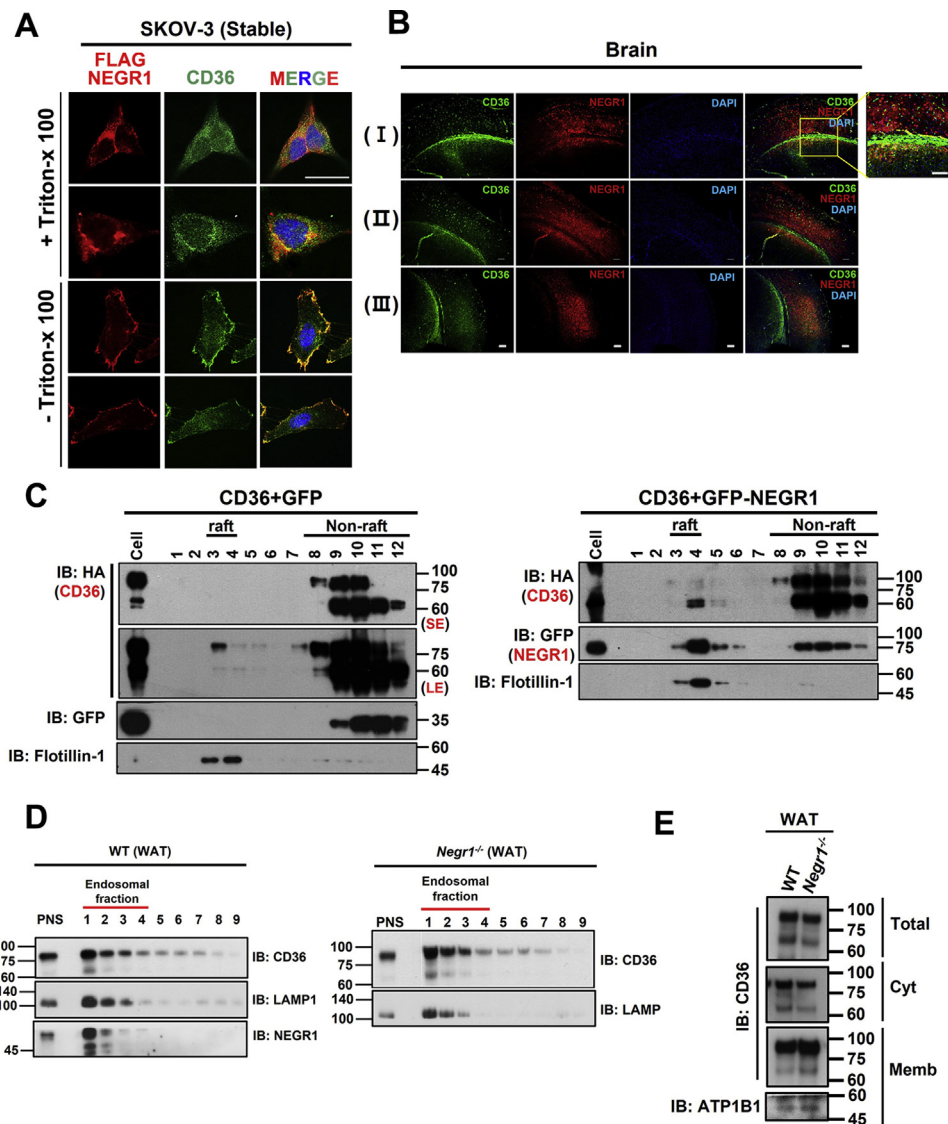


Fig. 4. NEGR1 was colocalized with CD36 in the plasma membrane. **A:** Immunofluorescence microscopy of SKOV-3-FLAG-NEGR1 stable cells. Cells were incubated with anti-FLAG (red) and anti-CD36 (green) antibodies, which was followed by incubation with anti-rabbit Cy3-conjugated and anti-mouse FITC secondary antibodies. Imaging was done using the Olympus BX51 microscope. Bar represents 50 μ m. **B:** Immunohistochemical analysis was performed using the paraffin-embedded brain tissue sections obtained from 13-week-old *Negr1*^{+/+} mice. Samples were immunostained with the anti-CD36 and anti-NEGR1 antibodies. Bar represents 50 μ m. **C:** Lipid raft fractionation was performed using 293T cells were transfected with HA-CD36 plasmid together with GFP control (left) or GFP-NEGR1 (right). Then, both samples were subjected to membrane fractionation by flotation method using OptiPrep™ gradient. CD36 and NEGR1 were visualized with anti-HA and anti-GFP antibodies, respectively. Flotillin-1 was used as a raft marker. **D:** Subcellular distribution of CD36 protein in WT and *Negr1*^{-/-} mice. Gonadal WATs were lysed and subjected to subcellular fractionation using OptiPrep™ density gradient. **E:** Plasma membrane isolation using WATs of WT and *Negr1*^{-/-} mice. ATP1B1, ATPase Na⁺/K⁺-transporting subunit beta 1; LE, long exposure; SE, short exposure.

(30 μ g/ml) after transfection into HeLa cells, in which only the mature forms of CD36 were dominant. CD36 degraded more rapidly upon NEGR1 coexpression (Fig. 5B), supporting that NEGR1 affects CD36 protein stability.

We also evaluated CD36 protein levels in 3T3-L1-NEGR1-FLAG stable cells (21) using an anti-CD36 antibody. The CD36 level of NEGR1-overexpressing 3T3-L1 cells was reduced by ~46% compared with that of control cells (Fig. 5C). Then, we examined NEGR1-deficient MEFs with or without preincubation in

0.1 mM oleic acid for 24 h. Although CD36 level increased in *NEGR1*^{-/-} MEFs regardless of the addition of oleic acid, the increase was less prominent than in the normal culture condition (Fig. 5D) indicating that NEGR1 may negatively regulate CD36 protein level.

We then examined CD36 protein level in the gonadal WAT of *Negr1*^{-/-} mice by immunoblotting. The CD36 protein level in *Negr1*^{-/-} mice increased by approximately 1.3-fold (Fig. 6A) compared with that in WT mice, as verified by immunostaining of WAT tissue sections with an anti-CD36 antibody (Fig. 6B). The CD36

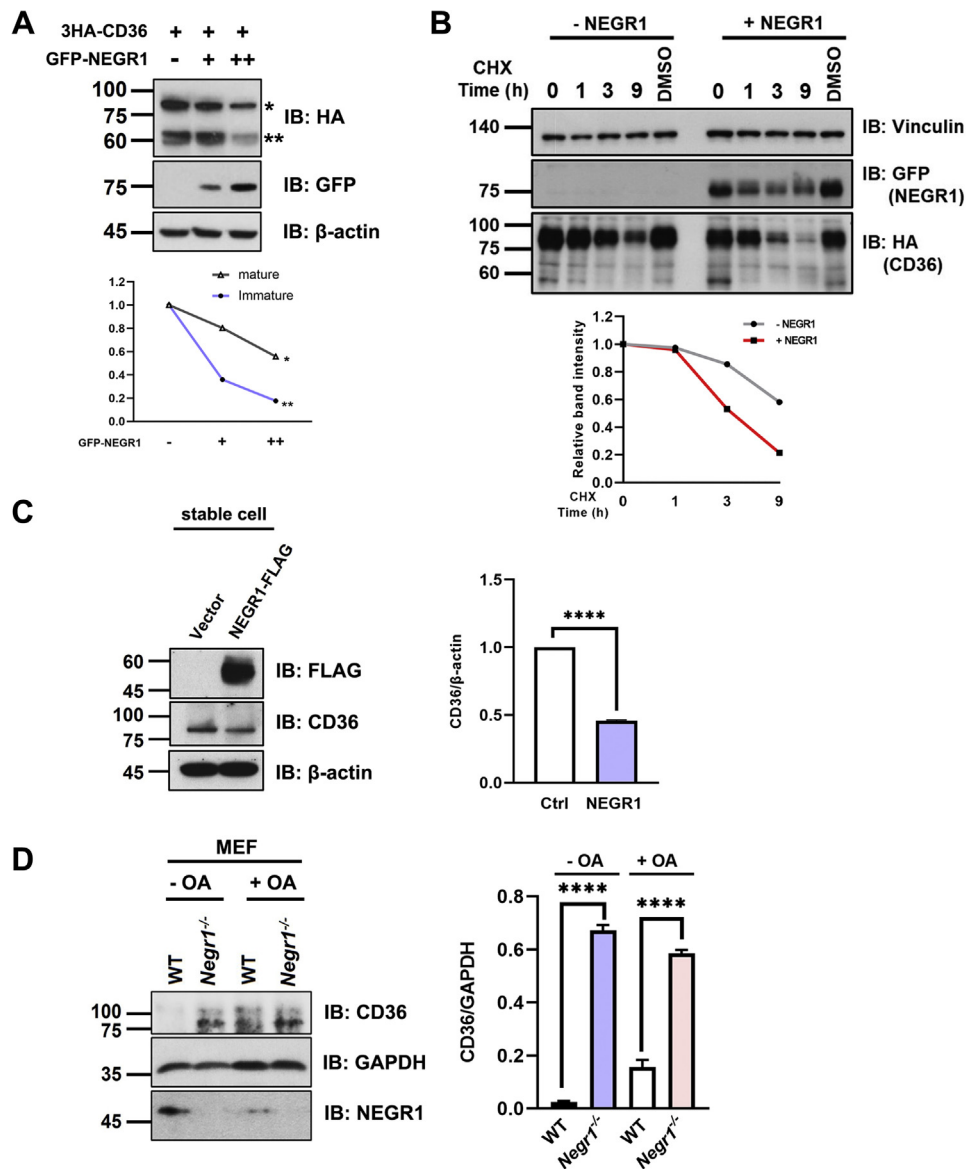


Fig. 5. NEGR1 expression may influence CD36 protein level. A: First, 293T cells were transfected with HA-CD36 together with increasing amounts of GFP-NEGR1 plasmids. Then, same amount of total protein (30 μ g) was loaded on SDS-PAGE, and CD36 proteins were detected using anti-HA antibody. Each CD36 band intensity in the image was quantified using ImageJ software. B: Determination of the half-life of CD36 protein. After HeLa cells were transfected with HA-CD36 with or without coexpression of GFP-NEGR1, cells were incubated with 30 μ g/ml cycloheximide (CHX) for the indicated times. C: Comparison of endogenous CD36 level in vector- or NEGR1-expressing 3T3-L1-NEGR1-FLAG stable cells. CD36 was detected by immunoblotting with anti-CD36, and the band intensity was quantified using ImageJ. D: Determination of CD36 protein level in WT and *Negr1*^{-/-} MEFs. WT and NEGR1-deficient MEFs were incubated either in the normal culture condition (oleic acid; - OA) or in the presence of 0.1 mM OA (+OA) for 24 h and subjected to immunoblotting. Endogenous CD36 and NEGR1 were visualized with the specific antibodies for each protein.

protein level in liver tissues of *Negr1*^{-/-} mice was also substantially elevated, as confirmed by immunoblotting (Fig. 6C) and tissue section staining (Fig. 6D). Western blotting showed that CD36 signals in *Negr1*^{-/-} mice were ~2.2-fold higher than those in WT mice. Collectively, our data demonstrated that CD36 protein levels were increased in NEGR1-deficient cells.

Fatty acid uptake and ROS levels in *NEGR1*^{-/-} MEFs

Based on the increased CD36 expression in NEGR1-knockout cells, we hypothesized that the high WAT weight exhibited by *NEGR1*^{-/-} mice (21) could be

linked to increased fatty acid transportation. To evaluate this, fatty acid uptake rates were determined for the primary adipocytes obtained from WT and *NEGR1*^{-/-} mice using a Free Fatty Acid Uptake Assay kit. Fluorescence signals were collected at each time point for 40 min. The final estimation showed that fatty acid uptake of NEGR1-deficient adipocytes was ~1.5-fold higher than that of WT controls ($P = 0.000008$, Fig. 7A). In addition, the primary adipocytes from WT and *NEGR1*^{-/-} mice were incubated with 0.1 mM oleic acid for 24 h, and their lipid droplets were visualized using BODIPY 493/503 staining. Adipocytes

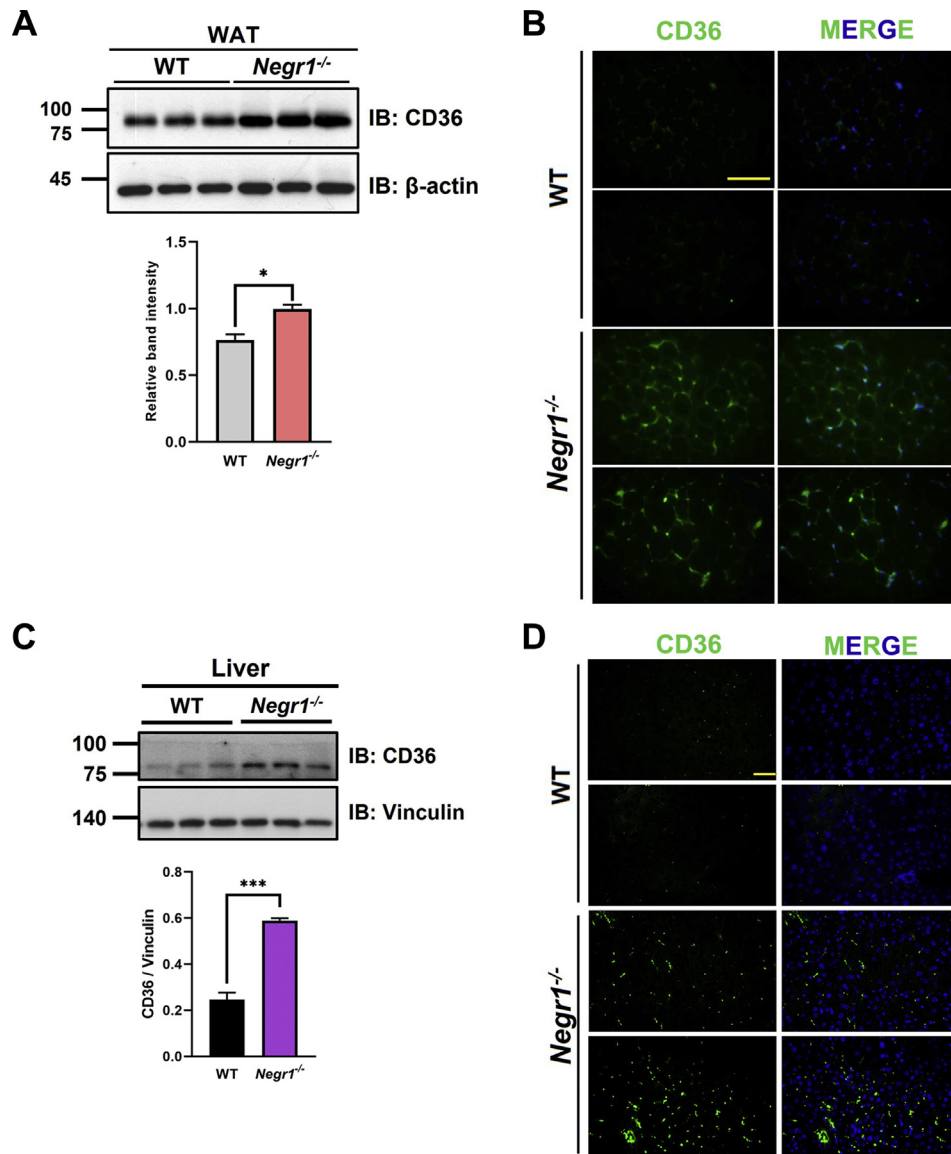


Fig. 6. CD36 protein levels in WAT and liver of *Negr1*^{-/-} mice. **A:** Epididymal fat tissues of 10-week-old WT and *Negr1*^{-/-} mice were obtained and used for the determination of CD36 protein level ($n = 6-8$). Immunoblotting was performed with anti-CD36 antibody, and intensities of both bands were quantified using ImageJ and normalized using the vinculin expression level. The data represent mean \pm SD. $**P < 0.01$. **B:** Immunohistochemical analysis was performed using the paraffin-embedded WAT tissue sections of the WT or *Negr1*^{-/-} mice. The tissue sections were incubated with the anti-CD36 antibody, and subsequent incubation with FITC anti-mouse secondary antibody. **C:** CD36 expression levels in the liver of the WT and *Negr1*^{-/-} mice ($n = 6-8$). Band intensities in Western blotting were determined using the ImageJ software. $***P < 0.001$. **D:** Comparison of CD36 expression in the liver tissue of WT and *Negr1*^{-/-} mice by using immunohistochemical analysis with anti-CD36 antibody. Imaging was done using an Olympus BX51 microscope. Bar represents 50 μ m.

from *NEGR1*^{-/-} mice showed higher lipid content than those from WT mice (Fig. 7B) revealing that *NEGR1*-deficient cells showed increased fatty acid uptake and/or storage.

Considering that fatty acid utilization is often associated with cellular oxidative stress generation, we examined ROS levels in WT and *NEGR1*^{-/-} MEFs using a DCFDA/H₂DCFDA Cellular ROS Assay kit. Although the ROS levels of WT and *NEGR1*^{-/-} MEFs were not different under normal conditions, the ROS level of *NEGR1*^{-/-} MEFs increased more than that of WT cells after the addition of H₂O₂ (Fig. 7C). The difference was

gradually intensified with increasing concentrations of H₂O₂, showing a ~ 1.2 -fold increase after the addition of 150 mM H₂O₂ ($P = 0.00002$). Similarly, ROS production of *NEGR1*^{-/-} MEFs increased more severely with the addition of oleic acid to the culture media (Fig. 7D), suggesting that *NEGR1*-deficient cells have higher levels of oxidative stress.

Finally, given that AMPK activation is closely associated with fatty acid utilization and cellular oxidative stress (30), we examined the activation of AMPK in *NEGR1*^{-/-} MEFs. Under normal culture conditions, p-AMPK levels in *NEGR1*-deficient cells were lower

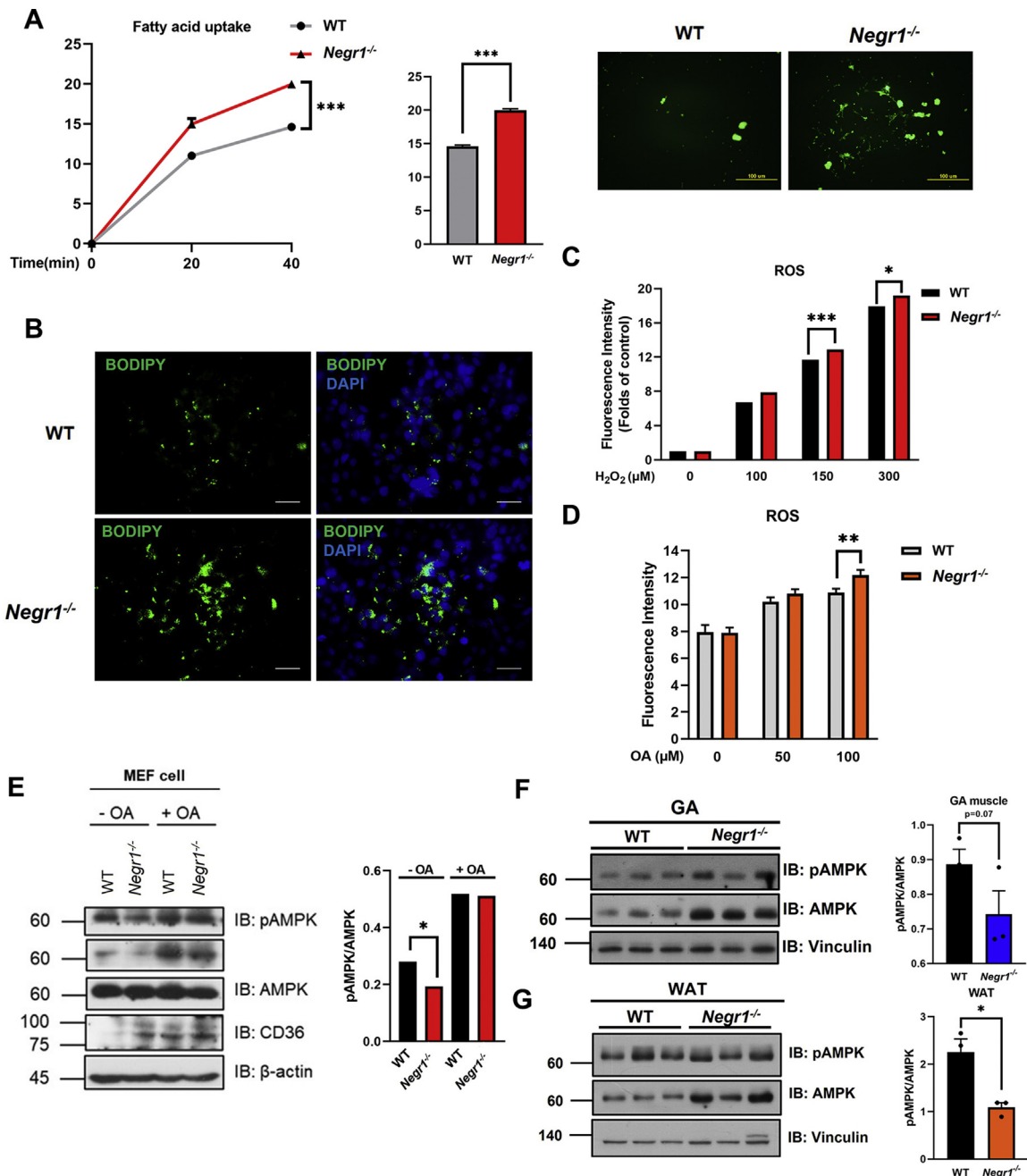


Fig. 7. Determination of fatty acid uptake rate and cellular ROS level. **A:** Fatty acid uptake rate was measured with a Free Fatty Acid Uptake Assay kit using primary adipocytes from gonadal fat tissue of WT and *Negr1*^{-/-} mice. Fluorescence signals were measured until 40 min using a fluorescence microplate reader FlexStation 3 at 485/515 nm. All experiments were performed in triplicates, and the data are presented as the mean ± SD. Imaging was performed using an Olympus BX51 microscope. Bar represents 100 μm. **B:** After primary adipocytes obtained from WT and *Negr1*^{-/-} mice were incubated with 0.1 mM oleic acid for 24 h, cells were subjected to BODIPY 493/503 staining. Bar represents 50 μm. **C** and **D:** Cellular ROS levels of WT and *Negr1*^{-/-} MEFs were measured using DCFDA/H2DCFDA Cellular ROS Assay kit. If necessary, cells were preincubated with H₂O₂ (**C**) or oleic acid (**D**) for 24 h. Fluorescence signals were measured at 485/515 nm. **E:** Activated AMPK levels in WT and *Negr1*^{-/-} MEFs. AMPK and p-AMPK levels were detected by immunoblotting after cells were incubated for 24 h in the presence or absence of 0.1 mM oleic acid. **F** and **G:** AMPK activation levels in GA muscle (**F**) and gonadal WAT (**G**) obtained from 10-week-old WT and *Negr1*^{-/-} mice (*n* = 6). **P* < 0.05.

than those in WT cells, despite the elevated CD36 protein levels in these cells (Fig. 7E). After incubation with 0.1 mM oleic acid, both CD36 and p-AMPK levels were upregulated. However, the activated AMPK level was still lower in *NEGR1*^{-/-} MEFs than in WT cells, which was inversely correlated with CD36 levels. In addition,

we examined p-AMPK levels in adipose and GA muscle tissues of *Negr1*^{-/-} and WT mice. In both tissues, the ratio of p-AMPK/AMPK decreased in *Negr1*^{-/-} mice compared with that of WT mice, which is consistent with the p-AMPK results for *Negr1*^{-/-} MEF cells (Fig. 7F, G). Collectively, our data suggest that AMPK activation

was attenuated in NEGRI-depleted cells, despite the increased oxidative stress.

DISCUSSION

CD36 is a multifunctional scavenger receptor that functions as a modulator of lipid homeostasis and immune response (31). The cellular fatty acid uptake rate is controlled primarily by the amount of CD36 protein on cellular membranes (7). CD36 fulfills a variety of functions depending on its tissue location. In the cardiac and skeletal muscles of humans, CD36 is recognized as a major fatty acid transporter that supplies cells energy (31). In adipocytes, CD36 mainly contributes to LCFA intake and regulates the process of lipid storage (32). CD36 is also considered a marker of human adipocyte progenitors, and high CD36 level implies high triglyceride accumulation potential (31).

In the present study, both mRNA and protein levels of CD36 were increased in the liver, brain, and adipose tissues of NEGRI-knockout mice (Figs. 1D and 6). Considering that CD36 plays key roles in LCFA uptake, our data were corroborated by the previously observed phenotypes of *Negr1*^{-/-} mice displaying high fat content in the liver and adipose tissues (21). Contrastingly, the mRNA level of CD36 in *Negr1*^{-/-} mice was down-regulated in the skeletal muscle (Fig. 1D) and was associated with the skeletal muscle atrophy and impaired exercise capacity of *Negr1*^{-/-} mice (21). Although it is widely known that peroxisome proliferator-activated receptor gamma increases CD36 expression in many tissues, its agonist modulates CD36 expression in a tissue-specific manner in diabetic rodents (33), suggesting a tissue-specific regulatory system in vivo. In addition, many reports have shown that exercise training decreased CD36 expression in muscle and adipose tissues (34, 35). In contrast, exercise training decreased CD36 expression in adipose tissues of insulin-resistant individuals (36), demonstrating that carbohydrate and lipid metabolism are mutually regulated. The prediabetic condition of *Negr1*^{-/-} mice evidenced in our previous study (21) might therefore be related to differences in the regulation of CD36 levels in different *Negr1*^{-/-} mice tissues.

CD36 is a member of an evolutionarily conserved protein family, which includes the high density lipoprotein scavenger receptor BI and LIMP-2 (29). The identification of the protein structure of LIMP-2 provided insight into predicting the structural features of CD36 (37). CD36 is an integral membrane protein that includes a hairpin-like structure with both N and C termini inside the cell (29). The predicted fatty acid binding pocket contains a stretch of hydrophobic residues (186–204) that may loop down to the cell membrane (29). In the present study, domain analysis revealed that the small N-terminal fragment (N1, 30–125) of CD36 was sufficient for interaction with NEGRI (Fig. 3B). Although a fragment containing the

hydrophobic patch (N2, 30–242) seemed to lose binding affinity, because of its low expression level, we hypothesized that the exposed hydrophobic region of N2 may destabilize the conformation of this region, which was overcome by the additional C-terminal region of N3. The six cysteine residues of N3 may contribute to stabilize the conformation of the extracellular region.

Mammalian AMPK is regarded as a sensor of cellular energy status that is activated by various cellular stresses including oxidative stress (30). As fatty acid uptake and oxidation are closely related, the activations of CD36 and AMPK are also related, although in diverse and conflicting ways. In the present study, the AMPK activation level of *Negr1*^{-/-} MEFs was lower than that of WT cells, despite the higher susceptibility of *Negr1*^{-/-} MEFs than that of WT cells to oxidative stress. Considering that CD36 expression suppresses AMPK activation in many cell types and that AMPK is constitutively activated in CD36-knockout mice (38), the elevated CD36 levels in *Negr1*^{-/-} cells could contribute to suppress AMPK activation. In adipocytes, AMPK activation induced by fasting and exercise promotes fatty acid oxidation to deplete cellular fatty acids (39). The high fat accumulation in *Negr1*^{-/-} adipocytes also corresponded with low AMPK activation.

As a scavenger receptor, CD36 binds and internalizes oxidized LDL in macrophages, which is pivotal in foam cell formation (40). Oxidized LDL was reported to induce the expression of effectors of LCFA uptake and mitochondrial ROS production (41). Furthermore, it was proposed that serum fatty acid levels can be important predictors of serum cholesterol concentration (42), suggesting some degree of correlation between fatty acid and cholesterol levels. In a previous study, we found that NEGRI is involved in cholesterol transport by interacting with the Niemann-Pick disease type C 2 protein, which functions critically in intracellular cholesterol trafficking (20). CD36 expression has been reported to be upregulated in Niemann-Pick disease type C 2-null human fibroblasts (43). Thus, our new findings on the NEGRI-CD36 association may be useful for identifying a potential target for controlling intracellular fatty acid and cholesterol levels.

Brain tissues are rich in lipids and fatty acids, which have been associated with many neurodegenerative diseases and mental disorders (44). Cholesterol is essential for neuronal physiology, and altered brain cholesterol homeostasis has been implicated in many neuropathological conditions (45). Evidence has been accumulated on the potential role of CD36 in CNS-related human disorders, and CD36 is reported to act as a scavenger receptor for amyloid fibrils to promote ROS (46). Furthermore, studies have revealed that cellular CD36 levels are related to anxiety (47) and depression (48), indicating that dysregulation of CD36 is associated with important psychiatric conditions in humans. Therefore, our findings may contribute to

deciphering the role of NEGR1 and CD36 in the regulation of brain lipid composition and development of psychiatric disorders in humans.

Data availability

The data presented in this study are available from the corresponding author upon reasonable request. 

Supplemental data

This article contains [supplemental data](#).

Acknowledgments

The authors are thankful to the National Research Foundation of Korea grants, NRF-2020R1A2C20112881I and NRF-2020R1A5A8017671, funded by the Korean government (Ministry of Science and ICT) for supporting this work.

Author contributions

Y. J. methodology; A. Y. investigation; S. J. L. resources; Y. C. data curation; S. L. writing—original draft; A. Y. visualization; S. L. supervision; S. L. funding acquisition.

Author ORCIDiDs

Yeongmi Cheon  <https://orcid.org/0000-0001-8986-9308>

Soojin Lee  <https://orcid.org/0000-0002-0383-5025>

Conflict of interest

The authors declare that they have no conflicts of interest with the contents of this article.

Abbreviations

AMPK, adenosine monophosphate-activated protein kinase; CD36, cluster of differentiation 36; FABPpm, plasma membrane fatty acid-binding protein; FATP, fatty acid transporter protein; GA, gastrocnemius; GST, glutathione-S-transferase; HA, hemagglutinin; H₂O₂, hydrogen peroxide; IP, immunoprecipitation; LCFA, long-chain fatty acid; MEF, mouse embryonic fibroblast; NEGR1, neuronal growth regulator 1; p-AMPK, phosphorylated AMPK; PLA, proximity ligation assay; ROS, reactive oxygen species.

Manuscript received October 8, 2021, and in revised from April 25, 2022. Published, JLR Papers in Press, May 6, 2022, <https://doi.org/10.1016/j.jlr.2022.100221>

REFERENCES

1. Unger, R. H., and Orci, L. (2000) Lipotoxic diseases of nonadipose tissues in obesity. *Int. J. Obes. Relat. Metab. Disord.* **24**, S28–32
2. Kopelman, P. G. (2000) Obesity as a medical problem. *Nature*. **404**, 635–643
3. Yao, C. H., Fowle-Grider, R., Mahieu, N. G., Liu, G. Y., Chen, Y. J., and Wang, R. (2016) Exogenous fatty acids are the preferred source of membrane lipids in proliferating fibroblasts. *Cell Chem. Biol.* **23**, 483–493
4. Doege, H., and Stahl, A. (2006) Protein-mediated fatty acid uptake: novel insights from in vivo models. *Physiology (Bethesda)*. **21**, 259–268
5. Su, X., and Abumrad, N. A. (2009) Cellular fatty acid uptake: a pathway under construction. *Trends Endocrinol. Metab.* **20**, 72–77
6. Mallick, R., Basak, S., and Duttaroy, A. K. (2021) Fatty acids and evolving roles of their proteins in neurological, cardiovascular disorders and cancers. *Prog. Lipid Res.* **83**, 101116
7. Glatz, J. F. C., and Luiken, J. (2018) Dynamic role of the transmembrane glycoprotein CD36 (SR-B2) in cellular fatty acid uptake and utilization. *J. Lipid Res.* **59**, 1084–1093
8. Hao, J. W., Wang, J., Guo, H., Zhao, Y. Y., Sun, H. H., Li, Y. F., et al. (2020) CD36 facilitates fatty acid uptake by dynamic palmitoylation-regulated endocytosis. *Nat. Commun.* **11**, 4765
9. Pohl, J., Ring, A., Korkmaz, U., Ehehalt, R., and Stremmel, W. (2005) FAT/CD36-mediated long-chain fatty acid uptake in adipocytes requires plasma membrane rafts. *Mol. Biol. Cell*. **16**, 24–31
10. Park, Y. M. (2014) CD36, a scavenger receptor implicated in atherosclerosis. *Exp. Mol. Med.* **46**, e99
11. Fentz, J., Kjobsted, R., Birk, J. B., Jordy, A. B., Jeppesen, J., Thorsen, K., et al. (2015) AMPKalpha is critical for enhancing skeletal muscle fatty acid utilization during in vivo exercise in mice. *FASEB J.* **29**, 1725–1738
12. Kim, H., Hwang, J. S., Lee, B., Hong, J., and Lee, S. (2014) Newly identified cancer-associated role of human neuronal growth regulator 1 (NEGR1). *J. Cancer*. **5**, 598–608
13. Willer, C. J., Speliotes, E. K., Loos, R. J. Li, S., Lindgren, C. M., Heid, I. M., et al. (2009) Six new loci associated with body mass index highlight a neuronal influence on body weight regulation. *Nat. Genet.* **41**, 25–34
14. Snickers, S., Stringer, S., Watanabe, K., Jansen, P. R., Coleman, J. R. I., Krapohl, E., et al. (2017) Genome-wide association meta-analysis of 78,308 individuals identifies new loci and genes influencing human intelligence. *Nat. Genet.* **49**, 1107–1112
15. Schizophrenia Working Group of the Psychiatric Genomics, C. (2014) Biological insights from 108 schizophrenia-associated genetic loci. *Nature*. **511**, 421–427
16. Hyde, C. L., Nagle, M. W., Tian, C., Chen, X., Paciga, S. A., Wendland, J. R., et al. (2016) Identification of 15 genetic loci associated with risk of major depression in individuals of European descent. *Nat. Genet.* **48**, 1031–1036
17. Ni, H., Xu, M., Zhan, G. L., Fan, Y., Zhou, H., Jiang, H. Y., et al. (2018) The GWAS risk genes for depression may be actively involved in Alzheimer's Disease. *J. Alzheimer's Dis.* **64**, 1149–1161
18. Noh, K., Lee, H., Choi, T. Y., Joo, Y., Kim, S. J., Kim, H., et al. (2019) Negrl controls adult hippocampal neurogenesis and affective behaviors. *Mol. Psych.* **24**, 1189–1205
19. Walley, A. J., Jacobson, P., Falchi, M., Bottolo, L., Andersson, J. C., Petretto, E., et al. (2012) Differential coexpression analysis of obesity-associated networks in human subcutaneous adipose tissue. *Int. J. Obes. (Lond)*. **36**, 137–147
20. Kim, H., Chun, Y., Che, L., Kim, J., Lee, S., and Lee, S. (2017) The new obesity-associated protein, neuronal growth regulator 1 (NEGR1), is implicated in Niemann-Pick disease Type C (NPC2)-mediated cholesterol trafficking. *Biochem. Biophys. Res. Commun.* **482**, 1367–1374
21. Joo, Y., Kim, H., Lee, S., and Lee, S. (2019) Neuronal growth regulator 1-deficient mice show increased adiposity and decreased muscle mass. *Int. J. Obes. (Lond)*. **43**, 1769–1782
22. Koh, W., Park, B., and Lee, S. (2015) A new kinetochore component CENP-W interacts with the polycomb-group protein EZH2 to promote gene silencing. *Biochem. Biophys. Res. Commun.* **464**, 256–262
23. Cheon, Y., Yoo, A., Seo, H., Yun, S. Y., Lee, H., Lim, H., et al. (2021) Na/K-ATPase beta1-subunit associates with neuronal growth regulator 1 (NEGR1) to participate in intercellular interactions. *BMB Rep.* **54**, 164–169
24. Cheon, Y., and Lee, S. (2018) CENP-W inhibits CDC25A degradation by destabilizing the SCF(beta-TrCP-1) complex at G2/M. *FASEB J.*, fj201701358RRR
25. Eyre, N. S., Cleland, L. G., Tandon, N. N., and Mayrhofer, G. (2007) Importance of the carboxyl terminus of FAT/CD36 for plasma membrane localization and function in long-chain fatty acid uptake. *J. Lipid Res.* **48**, 528–542
26. Luiken, J. J., Chanda, D., Nabben, M., Neumann, D., and Glatz, J. F. (2016) Post-translational modifications of CD36 (SR-B2): implications for regulation of myocellular fatty acid uptake. *Biochim. Biophys. Acta*. **1862**, 2253–2258
27. Nergiz-Unal, R., Rademakers, T., Cosemans, J. M., and Heemskerk, J. W. (2011) CD36 as a multiple-ligand signaling receptor

- in atherothrombosis. *Cardiovasc. Hematol. Agents Med. Chem.* **9**, 42–55
28. Tarhda, Z., Sendlali, O., Kettani, A., Moussa, A., Abumrad, N. A., and Ibrahim, A. (2013) Three dimensional structure prediction of fatty acid binding site on human transmembrane receptor CD36. *Bioinform. Biol. Insights*. **7**, 369–373
 29. Pepino, M. Y., Kuda, O., Samovski, D., and Abumrad, N. A. (2014) Structure-function of CD36 and importance of fatty acid signal transduction in fat metabolism. *Annu. Rev. Nutr.* **34**, 281–303
 30. Hardie, D. G., and Pan, D. A. (2002) Regulation of fatty acid synthesis and oxidation by the AMP-activated protein kinase. *Biochem. Soc. Trans.* **30**, 1064–1070
 31. Zhao, L., Varghese, Z., Moorhead, J. F., Chen, Y., and Ruan, X. Z. (2018) CD36 and lipid metabolism in the evolution of atherosclerosis. *Br. Med. Bull.* **126**, 101–112
 32. Rodrigue-Way, A., Caron, V., Bilodeau, S., Keil, S., Hassan, M., Levy, E., *et al.* (2014) Scavenger receptor CD36 mediates inhibition of cholesterol synthesis via activation of the PPARgamma/PGC-1alpha pathway and Insig1/2 expression in hepatocytes. *FASEB J.* **28**, 1910–1923
 33. Singh Ahuja, H., Liu, S., Crombie, D. L., Boehm, M., Leibowitz, M. D., Heyman, R. A., *et al.* (2001) Differential effects of rexinoids and thiazolidinediones on metabolic gene expression in diabetic rodents. *Mol. Pharmacol.* **59**, 765–773
 34. Smith, B. K., Bonen, A., and Holloway, G. P. (2012) A dual mechanism of action for skeletal muscle FAT/CD36 during exercise. *Exerc. Sport Sci. Rev.* **40**, 211–217
 35. Lehnig, A. C., Dewal, R. S., Baer, L. A., Kitching, K. M., Munoz, V. R., Arts, P. J., *et al.* (2019) Exercise training induces depot-specific adaptations to white and brown adipose tissue. *iScience*. **11**, 425–439
 36. Honkala, S. M., Motiani, P., Kivela, R., Hemanthakumar, K. A., Tolvanen, E., Motiani, K. K., *et al.* (2020) Exercise training improves adipose tissue metabolism and vasculature regardless of baseline glucose tolerance and sex. *BMJ Open Diabetes Res. Care*. **8**, e000830
 37. Neculai, D., Schwake, M., Ravichandran, M., Zunke, F., Collins, R. F., Peters, J., *et al.* (2013) Structure of LIMP-2 provides functional insights with implications for SR-BI and CD36. *Nature*. **504**, 172–176
 38. Samovski, D., Sun, J., Pietka, T., Gross, R. W., Eckel, R. H., Su, X., *et al.* (2015) Regulation of AMPK activation by CD36 links fatty acid uptake to beta-oxidation. *Diabetes*. **64**, 353–359
 39. Daval, M., Fougelle, F., and Ferre, P. (2006) Functions of AMP-activated protein kinase in adipose tissue. *J. Physiol.* **574**, 55–62
 40. Collot-Teixeira, S., Martin, J., McDermott-Roe, C., Poston, R., and McGregor, J. L. (2007) CD36 and macrophages in atherosclerosis. *Cardiovasc. Res.* **75**, 468–477
 41. Chen, Y., Yang, M., Huang, W., Chen, W., Zhao, Y., Schulte, M. L., *et al.* (2019) Mitochondrial metabolic reprogramming by CD36 signaling drives macrophage inflammatory responses. *Circ. Res.* **125**, 1087–1102
 42. Crowe, F. L., Skeaff, C. M., Green, T. J., and Gray, A. R. (2006) Serum fatty acids as biomarkers of fat intake predict serum cholesterol concentrations in a population-based survey of New Zealand adolescents and adults. *Am. J. Clin. Nutr.* **83**, 887–894
 43. Csepeggi, C., Jiang, M., Kojima, F., Crofford, L. J., and Frolov, A. (2011) Somatic cell plasticity and Niemann-Pick type C2 protein: fibroblast activation. *J. Biol. Chem.* **286**, 2078–2087
 44. Hussain, G., Schmitt, F., Loeffler, J. P., and Gonzalez de Aguilar, J. L. (2013) Fattening the brain: a brief of recent research. *Front. Cell Neurosci.* **7**, 144
 45. Martin, M. G., Pfrieger, F., and Dotti, C. G. (2014) Cholesterol in brain disease: sometimes determinant and frequently implicated. *EMBO Rep.* **15**, 1036–1052
 46. Coraci, I. S., Husemann, J., Berman, J. W., Hulette, C., Dufour, J. H., Campanella, G. K., *et al.* (2002) CD36, a class B scavenger receptor, is expressed on microglia in Alzheimer's disease brains and can mediate production of reactive oxygen species in response to beta-amyloid fibrils. *Am. J. Pathol.* **160**, 101–112
 47. Bakhshi Aliabad, M. H., Jafari, E., Karimi Kakh, M., Nosratabadi, R., Bakhshi, H., Sheikhha, M. H., *et al.* (2016) Anxiety leads to up-regulation of CD36 on the monocytes of chronic hepatitis B-infected patients. *Int. J. Psych. Med.* **51**, 467–475
 48. Bai, S., Wang, W., Wang, T., Li, J., Zhang, S., Chen, Z., *et al.* (2021) CD36 deficiency affects depressive-like behaviors possibly by modifying gut microbiota and the inflammasome pathway in mice. *Transl. Psych.* **11**, 16